Ozone-assisted oxidation of ethylene in a jet-stirred reactor: An experimental and modeling study

Caroline Smith Lewin, Olivier Herbinet, Frédérique Battin-Leclerc, Jérémy Bourgalais

Ozone-Assisted Oxidation of Ethylene in a Jet-Stirred Reactor: an Experimental and Modeling Study

Caroline Smith Lewin, Olivier Herbinet, Frédérique Battin-Leclerc, and Jérémy Bourgalais*

Université de Lorraine, CNRS, LRGP, F-54000 Nancy, France.

*Corresponding author: Jérémy Bourgalais

e-mail: jeremy.bourgalais@cnrs.fr

ORCID: 0000-0003-4710-8943

Phone: (33)3-72-74-38-17

KEYWORDS

Ozonolysis; Jet-stirred reactor; mass-spectrometry; gas chromatography; kinetic model

ABSTRACT

Ozone addition is a promising method to achieve improvement and control of combustion/ignition processes due to ozone-derived chemistry. However, the complexity induced by ozonolysis reactions make investigations on O_3-assisted oxidation with alkenes still scarce. In this work, the ozone-assisted oxidation of ethylene was studied in a jet-stirred reactor from 300 to 1000 K. The main products were identified and quantified by mass spectrometry/gas chromatography analysis. The mole fractions were then compared to those computed with a kinetic model from the literature. This work provides data for the development of detailed chemical kinetic models relevant to atmospheric and combustion chemistry studies.

INTRODUCTION

The so-called ozonolysis process during the gas-phase oxidation of organic compounds in presence of ozone (O_3) has been the subject of numerous studies for over a century in different scientific fields. The exothermic 1,3-dipolar cycloaddition of O_3 reaction onto unsaturated volatile organic compounds leads to the formation of reactive species called Criegee intermediates through a three-step mechanism [1,2]. Criegee intermediates affect the oxidative capacity of the atmosphere by being both a direct source of oxygenated compounds and radicals and by reacting with other species to form low-volatility compounds leading to the growth of aerosols and particles that impact the radiation balance and air quality (e.g., [3–6]). O_3-assisted oxidation of hydrocarbons is also a subject of recent interest in low-temperature combustion studies due to the recent rise of investigations into non-equilibrium plasma-assisted combustion techniques and chemically controlled engine designs for emission control and efficiency enhancement [7–11]. Efficiently generated by electric discharge, O_3 is a low-temperature reaction promoter and an enhancer of combustion processes through the formation of various reactive intermediates [12–14]. This enhancement is related to O_3 chemistry, with the production of oxygen atoms from the thermal decomposition of O_3 at elevated temperatures accelerating the overall chain-propagating process, as well as the rapid exothermic ozonolysis reactions initiating direct reactions

between fuel and O_3 at low temperatures (even at room temperature). While the direct reaction between O_3 and saturated hydrocarbons is almost negligible, the nearly barrierless reaction with unsaturated species (a difference of several orders of magnitude [15]) is very fast. Although considerable studies have been conducted on O_3-assisted oxidation of alkanes [16–23], investigations on alkenes are scarce, partially due to the much higher chemical complexity induced by these ozonolysis reactions.

Most ozonolysis reactions involve the formation of a primary cyclic 1,2,3-trioxy ozonide (POZ) from the van der Waals O_3-alkene complex resulting from the addition of O_3 onto the C=C bond. POZ then decomposes to form a carbonyl compound ($R_1R_2C=O$) and carbonyl oxide (R_3R_4COO), the famous Criegee intermediate (CI), via homolytic cleavage of C-C and C-O bonds (see FIGURE 1). After that, the quenching processes of the Criegee intermediate give access to many reaction pathways, such as the formation of 1,2,4-trioxy cyclic secondary ozonide (SOZ) [24–31]. A single O-O bond of the POZ can also break to give a POZ biradical, making the accessible kinetic networks even more complicated [32,33]. For recent reviews of CI's reaction pathways, readers may refer to Osborn & Taatjes [34] and Taatjes [35].

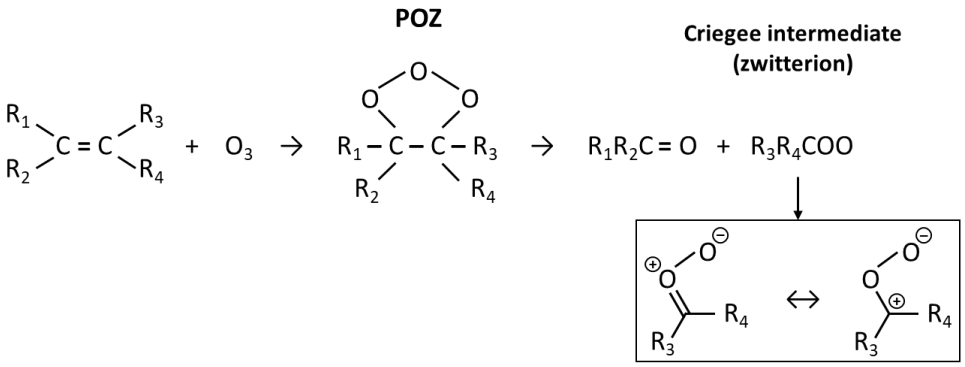

FIGURE 1. Formation of POZ and Criegee intermediate from ozonolysis reaction.

Due to the multiplicity of kinetic pathways involved in ozonolysis, grey areas remain even in the chemistry of the simplest O_3-alkene system. The chemical pathways following the reaction of O_3 with ethylene (CH_2=CH_2), despite being extensively studied for decades (see [36–41] for the most recent studies) are still not fully understood and significant disagreements remain between quantitative experiments and kinetic model predictions. The most recent quantitative investigation on the O_3-assisted oxidation of C_2H_4 was reported by

Rousso et al. [39]. The oxidation of C_2H_4 was carried out in a near atmospheric pressure (933 mbar) jet-stirred reactor (JSR) from 300 to 1000 K by adding 1000 ppm of O_3. The mole fraction as a function of temperature of the oxidation products were obtained by electron-ionization mass spectrometry analysis. Their data were compared to the predictions of a kinetic model developed at Princeton [42–44], in which ozonolysis reactions were described using global reactions based on IUPAC recommendations. They reported significant discrepancies between the experimental data and the predictions, even for the consumption of C_2H_4 and O_3, from low to intermediate temperatures (< 700 K) suggesting missing major reaction pathways in the kinetic model. However, no mechanistic insight has been provided and many questions remain regarding the formation pathways of intermediates in this system.

The aim of this work is to focus on the mostly unknown kinetic networks initiated by ozonolysis reactions over a wide temperature range. While O atoms from the O_3 thermal decomposition are of interest in lowering the fuel conversion temperature, ozonolysis can initiate alkene-based fuel conversion at even lower temperatures and may have an impact on auto-ignition [45]. In this work, new experimental data are generated over a wider range of experimental conditions for the O_3-assisted oxidation of C_2H_4 to confront the predictions of current kinetic models. Especially, due to a different experimental configuration, the newly obtained data shows that a global ozonolysis mechanism can accurately simulate the mole fractions of the main products as well as the consumption of C_2H_4 and O_3. The O_3-assisted oxidation of C_2H_4 was carried out in a JSR between 300 K and 1000 K with varying the mole fraction of O_3 from 1000 to 2000 ppm. The identification and the quantification of the main products and stable intermediates were performed by gas chromatography with mass spectrometry, thermal conductivity and flame ionization detections, and the obtained mole fractions were recorded as a function of temperature. The experimental data were then confronted to the predictions of the abovementioned kinetic model from the literature [42–44] to provide mechanistic insights into the O_3-assisted oxidation of C_2H_4.

EXPERIMENTAL SETUP

The experimental setup used in this work has been extensively described in the past, see for instance Bourgalais et al. [46], and only the essential information and modifications for the current experiments are given here. Constant pressure, residence time, and equivalence ratio of 1.067 bar, 2.5 s, and 0.5, respectively, were maintained for all the

experiments, with a continuous flowing gas mixture with mole fraction of 0.02 ethylene, 0.12 O_2, and 0.86 He in the JSR using calibrated Bronkhorst mass flow controllers (relative uncertainty of 0.5%). He and O_2 are provided by Messer (both 99.999% pure) and C_2H_4 by Air Liquide with a purity of 99.95%. A JSR temperature range from 300 to 1000 K was investigated and the flow rates were adjusted to maintain a constant nominal residence time. A preheating zone upstream of the JSR inlet ensured the temperature gradient inside the vessel to be limited. The annular quartz tube has an approximate cross section of 0.25 cm^2 and a length of 12 cm. The tube, as well as the JSR, is heated using THERMOCOAX resistances. To provide progressive preheating, its length is divided into two heating stages (6 cm long each) that are set to two different temperatures. For experiments without O_3, the preheaters were set to temperatures close to the desired temperature in the JSR. However, for O_3-assisted oxidation experiments, this procedure was followed only below the JSR temperature of 425 K, which is the threshold for the onset of O_3 thermal decomposition (as will be discussed later). From this temperature, to prevent O_3 decomposition before entering the reactor, the first preheater was set to 353 K and the second to 393 K, regardless of the JSR temperature. The reactor temperature was measured with a K-type thermocouple positioned in a glass finger close to the JSR center with an uncertainty of around 1%.

The C_2H_4 ozonolysis experiments were achieved adding an O_3 mole fraction of 1000 and 2000 ppm using an ozone generator (BMT 802N). Gas feeds of C_2H_4 and O_3 were mixed just before entering the preheated zone of the JSR (see FIGURE 2 for a scheme of the experimental setup). An ozone analyzer (BMT 965 ST) based on a dual-beam UV photometer at 254 nm was used at the exit of the JSR to measure the O_3 mole fraction. The uncertainty of 15% for the measurement of the O_3 mole fraction was derived including accuracy and repeatability error.

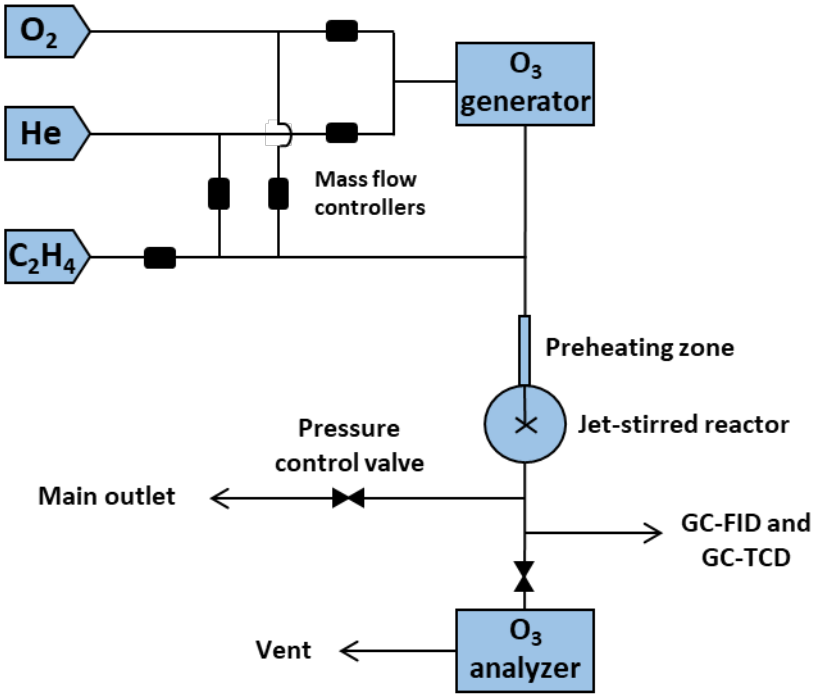

FIGURE 2. Scheme of the experimental setup.

C_2H_4 and its oxidation products were quantified using two gas chromatographs (GCs) connected to the exit of the JSR, one with a carbosphere-packed column and a thermal conductivity detector (TCD) to quantify lightweight and permanent gas species, the second with a Q-Bond capillary column and a flame ionization detector (FID) preceded by a methanizer for the quantification of organic compounds. For species identification, a GC equipped with a Q-Bond capillary column was coupled to a quadrupole mass spectrometer. Ions were generated via electron impact ionization at 70 eV. The mole fractions of species detected with the FID were calibrated using the effective carbon number (ECN) method. Their calibration factors were deduced from that of C_2H_4 by taking into account their effective carbon number. The relative uncertainties in their mole fractions were estimated to be ±10%. The obtained carbon balance presented values from 87.8 to 107.0%, with an average of 99.6%

KINETIC MODEL

An up-to-date kinetic model developed at Princeton coupling an ethylene oxidation mechanism and an O_3 sub-mechanism was used to simulate the experimental data [42–44]. Based on IUPAC recommendation (https://iupac.org/), the following direct reactions between O_3 and C_2H_4 were implemented to simulate global ozonolysis reactions:

$$O_3 + C_2H_4 \leftrightarrow CH_2O + OH + HCO \quad (1)$$

$$O_3 + C_2H_4 \leftrightarrow CH_2O + CO + H_2O \quad (2)$$

$$O_3 + C_2H_4 \leftrightarrow CH_2O + H + H + CO_2 \quad (3)$$

$$O_3 + C_2H_4 \leftrightarrow CH_2O + CO_2 + H_2 \quad (4)$$

Using the CHEMKINPro software [47], the oxidation of C_2H_4 without O_3 was modelled considering a perfectly stirred reactor (see results in FIGURE S1 in Supplementary Material) as it is usually the case when modelling JSR, since the residence time in the preheating zone is only a few percent of that in the JSR [48]. In the O_3-assisted oxidation case, two plug flow reactors (PFR) were included ahead of the JSR to simulate the experimental preheating zone composed of two heating stages. This strategy of including a PFR was also used by Rousso et al. [39]. This was performed to account for the reactivity, especially the O_3 thermal decomposition, before entering the JSR. The PFR simulations were based on the physical dimensions of the quartz tube from the entrance of the preheating zone to the JSR and utilizes the same temperature as used in the experiments. A numerical comparison between the composition at the outlet of the second PFR and that of the outlet of the JSR during O_3-assisted oxidation, as well as simulations using both reactor configurations (with and without PFRs), are presented in Supplementary Material. FIGURE S2 well demonstrates that a significant amount of O_3 enters the JSR. As it can be seen in FIGURE S3, a slightly improved agreement when PFRs were considered is observed. Flow rates used in each experiment were also implemented in the model and were provided as inputs of the PFRs.

RESULTS

As a starting point, oxidation experiments without O_3 addition were first conducted from 300 to 1000 K, as a reference for no low-temperature chemistry behavior. The evolution of the mole fractions of C_2H_4, O_2, the intermediates (CH_2O, C_3H_6, CH_3CHO, CH_4, and oxirane C_2H_4O), and the major products (CO and CO_2) as a function of temperature are given in FIGURE S1. No decrease in the mole fraction of C_2H_4 and O_2 is observed below 800 K in the absence of ozone. Note that H_2O is also predicted as a major product with a mole fraction comparable of those of CO and CO_2, but it remains difficult to quantify it accurately by GC analysis. Oxirane was detected with a maximum mole fraction of 130 ppm at 850 K and mainly formed from $HO_2 + C_2H_4$ by direct epoxidation. An overall good agreement between experimental data and simulations is observed even if a slight overestimation of the predicted conversion of C_2H_4 is

noticed between 800 and 850 K. At these temperatures, the conversion of C_2H_4 is mainly driven by addition of OH on C_2H_4, as can be observed in the flow rate analysis of FIGURE S4, at 900 K. The rate constants provided in the literature for this reaction and currently implemented in the kinetic model correspond to the formation of all the three C_2H_5O isomers (CH_2CH_2OH, OCH_2CH_3, and $HOCHCH_3$) [49]. This might result in a slight overestimation of CH_3CHO (see FIGURE S1). These results on the oxidation of neat C_2H_4 give confidence to the experimental setup and the analysis procedure used in this work.

Thermal decomposition of O_3 was also measured before considering the O_3-assisted oxidation of C_2H_4. O_3 mole fraction as a function of temperature was recorded at the same residence time and pressure as in the ozonolysis case but without C_2H_4, using as gas mole fractions: 0.12 O_2/0.001 O_3/0.879 He. FIGURE 3 presents the O_3 mole fraction as a function of temperature for neat O_3 thermal decomposition and for C_2H_4 oxidation with two O_3 mole fractions (1000 and 2000 ppm). Consistent with previous data in the literature [39,44,50], the thermal decomposition of O_3 starts ~450 K and ~90% of O_3 is consumed by 550 K. This result indicates that above this temperature, fuel interactions with O-atoms can potentially compete with ozonolysis reactions in the formation of intermediate species and products.

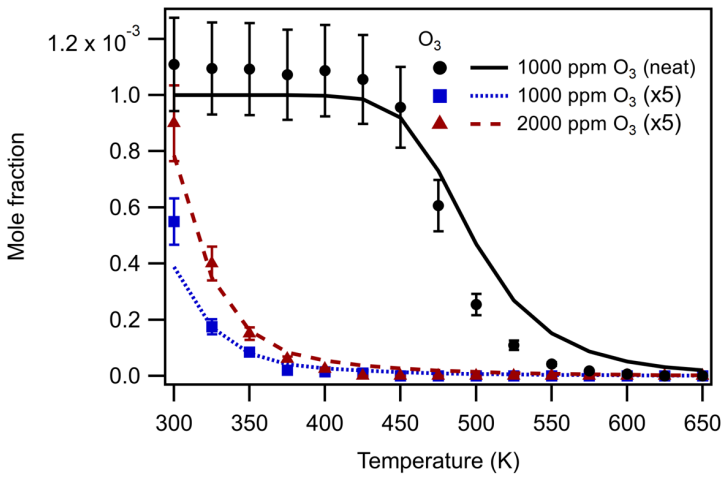

FIGURE 3. O_3 mole fraction as a function of temperature. Data in black correspond to the thermal decomposition of 1000 ppm of O_3 (without C_2H_4). Data in blue and red correspond to C_2H_4 oxidation with 1000 ppm and 2000 ppm of O_3, respectively. The markers refer to the experimental data and the lines to simulations.

Compared to neat O_3 thermal decomposition, O_3-assisted oxidation of C_2H_4 in FIGURE 3 shows that the addition of C_2H_4 induces a drastic shift of the O_3 consumption toward lower temperatures, with a consumption of ~90% of O_3 at 300 K and ~99% at 350 K. The simulations show a relatively good agreement for O_3 consumption for both mole fraction conditions. Increasing by a factor of two the mole fraction of O_3 in presence of C_2H_4 does not change the conversion yield of O_3.

FIGURE 4 shows that with the addition of O_3, the conversion of C_2H_4 starts since room temperature. A decrease in the mole fraction of C_2H_4, 4.5% and 9% respectively, compared to the initial mole fraction is observed at 300 K. Multiplying the mole fraction of O_3 by two leads to a twofold decrease of C_2H_4 at low temperatures. The C_2H_4 conversion is stable between 400 and 800 K, but decreases significantly from 850 K, indicating a transition to the high-temperature kinetic regime. No temperature shift is observed compared to the O_3-free experiments, but the conversion is more important (a factor of 5 at 850 K) when O_3 is added. This difference reduces as the temperature increases, until it becomes almost negligible at about 950 K. A similar onset of the high-temperature reactivity under different O_3-addition levels suggests that the addition of O-atom from the thermal decomposition of O_3 hardly alters the kinetics of the C_2H_4 oxidation above 800 K.

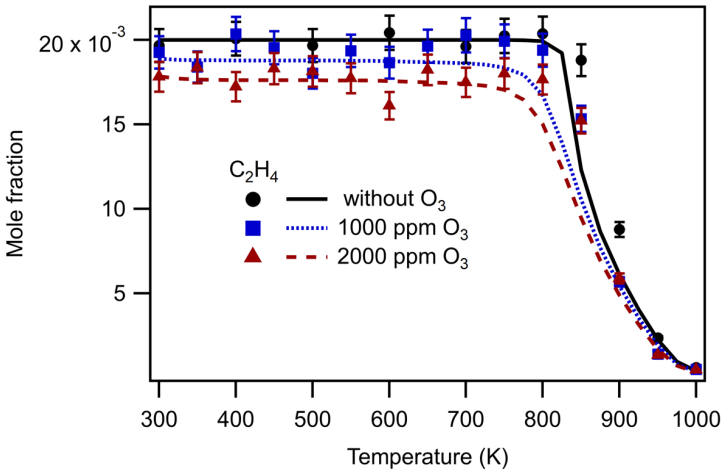

FIGURE 4. Consumption as a function of temperature of C_2H_4 diluted in a gas mixture made of O_2, O_3, and He. Two inlet mole fractions of O_3 have been used: 1000 (blue squares) and 2000 ppm (red triangles).

The simulation is in good agreement with the experimental data over all the temperature range. The model still slightly overestimates the conversion of C_2H_4 at high temperature, above 700 K. This discrepancy can be related to the overestimation of the reaction $C_2H_4 + HO_2$. A sensitivity analysis for C_2H_4 at 750 K (1000 ppm of O_3, see FIGURE S5) shows that the C_2H_4 mole fraction is mainly influenced by the reaction with HO_2. The formation of HO_2 is promoted by the O-atoms from the thermal decomposition of O_3. HO_2 is mainly produced from the H-abstraction of HCO by O_2 and HCO is originated from the reaction O + C_2H_4. FIGURE S6 shows the simulated mole fractions of O-atoms and OH radicals with and without O_3. The mole fraction of O-atoms increases below 600 K in agreement with the thermal decomposition of O_3 (see FIGURE 3) and reaches a plateau around 650 K, matching with the increase of the mole fraction of OH. The mole fractions of O-atoms and OH radicals when O_3 is added gradually join the mole fractions of O-atoms and OH when no O_3 is added from 800 K. The stability of the fuel mole fraction from room temperature up to 600 K shows that there is no significant impact of the thermal decomposition of O_3 on the C_2H_4 reactivity. The conversion of C_2H_4 is not affected by potential competition from O-derived chemistry. Flow rate analyses were performed at 350 and 650 K for the 1000 ppm of O_3 case (see FIGURES S8 and 5). At 650 K, the decomposition of O_3 into O-atoms corresponds to 52% of the total O_3 consumption.

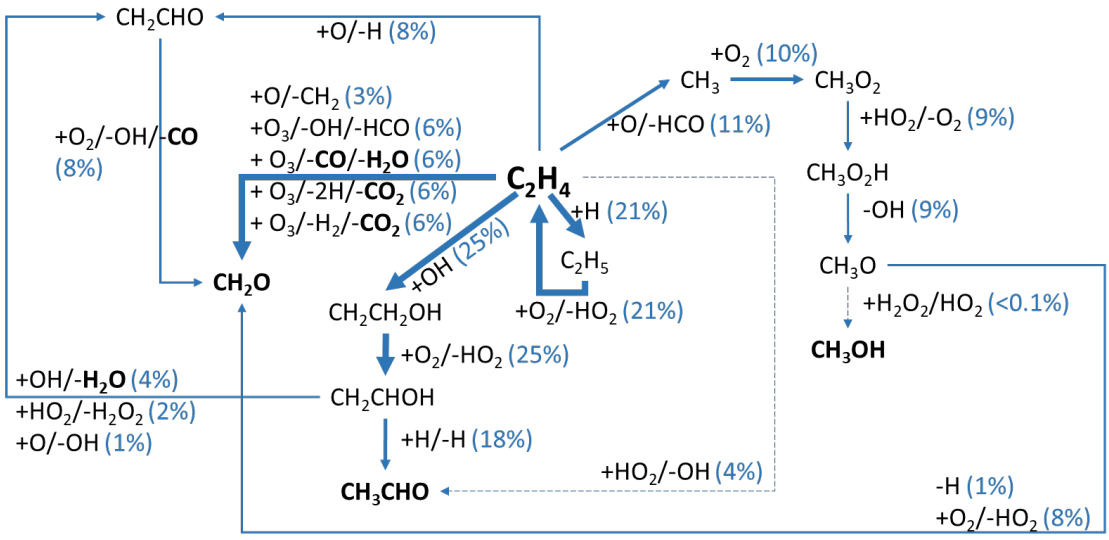

FIGURE 5. Flow rate analysis for C_2H_4 oxidation assisted by O_3 (1000 ppm) at 650 K obtained by simulations. Each arrow denotes the percentage of the corresponding pathway.

The good agreement observed in this work between simulation and experiments for the conversion of C_2H_4 deviates from the work of Rousso et al. [39], who showed a poor agreement between experiments and simulation. Rousso et al. observed experimentally a decrease of the C_2H_4 conversion as the temperature increased around 500 K. This increase of the C_2H_4 mole fraction, however, does not seem to have any chemical explanation and might be due to the thermal decomposition of O_3 in the injection line, as in their experimental setup O_3 and C_2H_4 are injected through two separate heated lines into the JSR. The effect of the thermal decomposition of O_3 is also reflected in Rousso et al. [39]'s profile of formaldehyde, which is the major product at low temperatures, and whose mole fraction drops to 0 between 500 – 800 K in their study. Based on the global reactions implemented in the model to describe the ozonolysis process, a 1:1 mole fraction of CH_2O:C_2H_4(consumed) is expected, but was not observed from 500 K by Rousso et al. [39]. In the present work, all gas lines were mixed before entering the preheating zone upstream of the reactor, in contrast to the separate injection of O_3 and C_2H_4 in Rousso et al. [39]'s work. As shown in FIGURE 6, a similar agreement between simulation and experiments as for C_2H_4 was found for CH_2O with a CH_2O:C_2H_4(consumed) mole fraction ratio of 1:1. To be sure about the mentioned bias in the experiments of Rousso et al. [39], additional experiments and simulations have been done using a similar injection configuration. Similar profiles for C_2H_4 and CH_2O as those of Rousso et al. [39] have been found (see FIGURE S7).

As is shown in FIGURE 6, a similar agreement between simulations and experiments as for C_2H_4 can be observed for the mole fraction profile of the main products, CH_2O, CO, and CO_2. At the lowest temperatures, CH_2O is the main product formed by the ozonolysis of C_2H_4. At 350 K and in the case of 1000 ppm of O_3, the mole fraction of CH_2O is about 800 ppm, which is twice the mole fraction of CO and CO_2. At 800 K, the mole fractions of CO and CH_2O are equivalent (around 1000 ppm). CH_2O, CO, and CO_2 are formed through the global reactions implemented in the kinetic model to describe ozonolysis (see FIGURE S8/equations 1 to 4). Those reactions allow to fairly well reproduce the mole fraction profiles of the main products. In the case of 2000 ppm of O_3, however, CH_2O is overestimated by up to ∼50%, indicating needed refinements in the considered product formation pathways. Water is also one of the major expected products at low temperatures, but as for the O_3-free experiments, it could not be quantified in this work. The predicted mole fraction of water is ∼250 ppm (see FIGURE S9).

Note that a 2-fold increase in the mole fraction of O_3 leads to an approximately 2-fold increase in the mole fraction of major products at low temperatures.

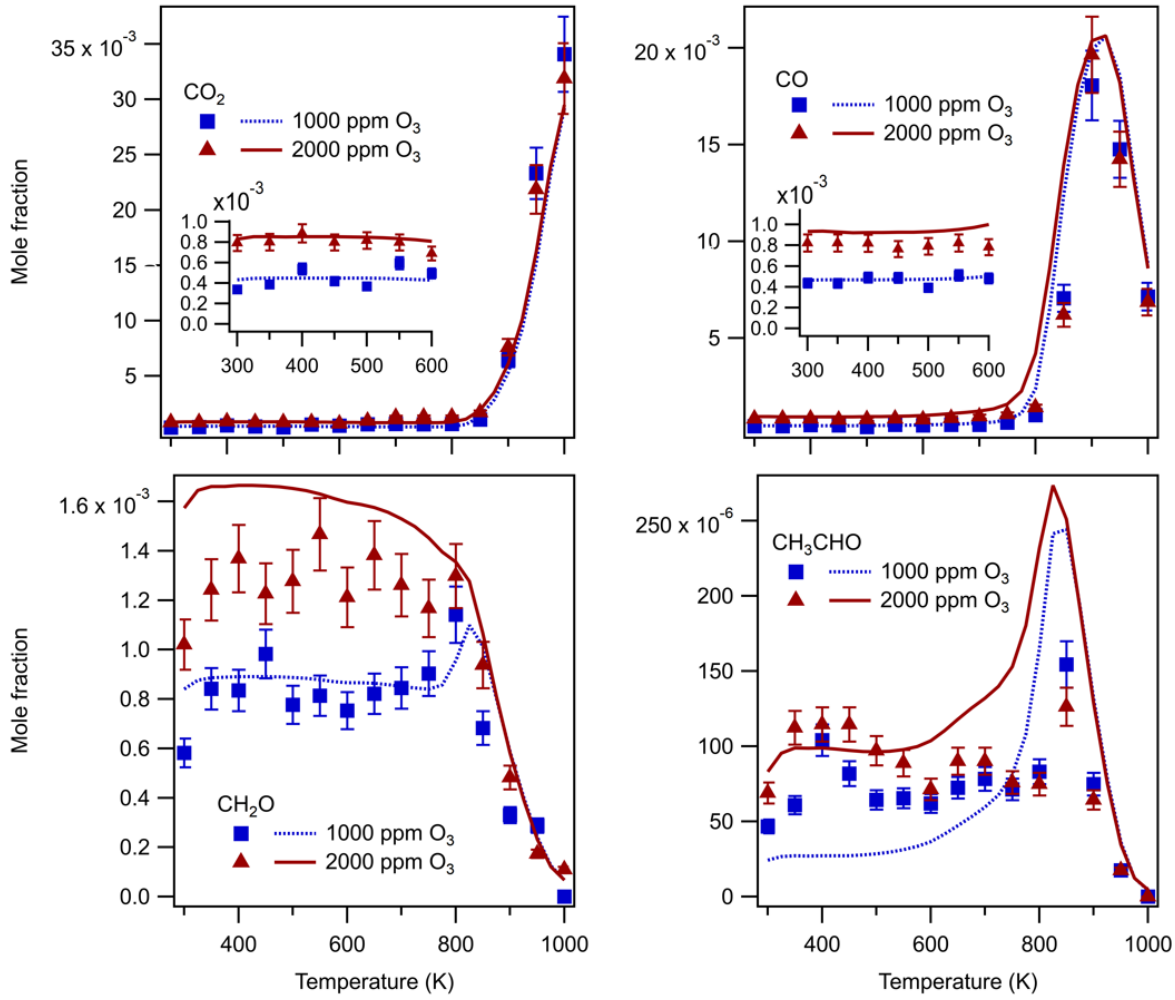

FIGURE 6. Comparison of experimental and predicted mole fractions as a function of temperature of low-temperature products measured during the O_3-assisted oxidation of C_2H_4. The symbols correspond to the experimental results and the lines to the predictions of the kinetic model.

Two minor products were also detected, acetaldehyde (see FIGURE 6) and oxirane (see FIGURE S10). Concerning CH_3CHO, discrepancies between experiments and simulations can be observed with overestimation up to a factor of two above 600 K. For 2000 ppm of O_3, the experimental data show a stable formation of CH_3CHO up to 800 K while the simulated mole fraction profile starts increasing from 600 K. The flow rate analysis at 650 K (see FIGURE 5) shows that the discrepancies at high temperature are still linked to the overestimation of the

315 reaction C_2H_4 + OH. The main fate of the CH_2CH_2OH radical coming from the addition reaction
316 C_2H_4 + OH is an H-abstraction by O_2 leading to ethenol (CH_2CHOH). Note that according to the
317 literature, ethenol has never been observed so far in GC and thus was not observed in this
318 work either, probably due to a fast tautomerization into CH_3CHO. In the 1000 ppm O_3 case,
319 experiments display a local maximum mole fraction located at 400 K, which is not reproduced
320 by the model.

321 Concerning oxirane, simulation also underestimates the mole fraction at the lowest
322 temperatures. The simulated profile starts to increase only above 550 K, while the
323 experimental data show a stable formation of about 12 ppm from 400 K and 500 K for both
324 initial O_3 concentrations. The mole fraction of oxirane is fairly well reproduced at higher
325 temperatures.

326 The underestimation of the production of the two minor products at low temperature
327 shows missing reaction pathways in the kinetic model. The reaction mechanisms should
328 therefore be more detailed than the global ozonolysis reactions that are currently
329 implemented in the kinetic model. The formation of oxirane observed at low temperatures
330 can be explained by the 1,2,3-trioxy ozonide (POZ) biradical decomposition giving oxirane and
331 singlet oxygen as proposed in the literature but the exit channel with the formation of oxygen
332 atom is predicted to be minor due to a higher energy barrier. Alternatively, the reaction
333 between CI and C_2H_4 can also be a source of oxirane with formaldehyde as co-product. The
334 measurement of the oxirane mole fraction profile in this work will provide a constraint for
335 future implementation of the kinetic parameters of the POZ biradical decomposition.
336 Moreover, a potential missing source for acetaldehyde could be the dissociation of the
337 hydroxymethyl formate ($HOCH_2OHCO$), coming from the isomerization of the POZ, through a
338 C-O bond rupture.

339 Methanol was also detected in smaller amounts than CH_2O, CO, and CO_2 since 300 K
340 in the 2000 ppm O_3 case but with a higher mole fraction than CH_3CHO and oxirane (see FIGURE
341 S10). In the 1000 ppm O_3 case, methanol only starts at 550 K. Above this temperature, both
342 profiles seem relatively similar. The mole fraction of methanol in both O_3 cases oscillates
343 between 30 and 70 ppm with a maximum around 700-750 K and is no longer detected above
344 850 - 900 K. The shape of the simulated mole fraction profile is relatively similar to the
345 experimental one at the highest temperatures, but with an order of magnitude lower and with
346 a ~90 K temperature shift. This temperature range fits with the formation of O-atoms (see

FIGURE S6). The flow rate analysis at 650 K (see FIGURE 5) shows that the main source of methanol is the reaction C_2H_4 + O leading to the formation of CH_3 with HCO. The main fate of CH_3 is the addition of O_2 to form CH_3OO and then methyl hydroperoxide (CH_3OOH). The formation of hydroperoxides following the reaction C_2H_4 + O_3 could not be addressed in this work due to their decomposition during the GC analysis but have been observed in the literature [39]. However, the formation of CH_3OH at low temperatures is not predicted by the kinetic model and the temperature range does not fit with the formation of O-atoms. The current formation of CH_3OH in the atmosphere is mainly due to the reactions of OH radical with CH_3 and CH_3OO [51,52], which are currently implemented in the kinetic model. This result shows that a reaction pathway is missing and that, as for CH_3CHO, CH_3OH would come from secondary reactions after the ozonolysis of C_2H_4.

Note that formic acid, HCOOH, has also been detected by GC-MS after condensation of the gas phase using a liquid nitrogen trap, but cannot be quantified since FID is not sensitive to formic acid. Its detection shows that it should be formed in notable amounts. As proposed by Neeb et al. [53], the production of HCOOH can occur via a bimolecular reaction between CIs and CH_2O, an important primary product at the lowest temperatures (see FIGURE 6).

CONCLUSION

The influence of the addition of O_3 on the oxidation of C_2H_4 was experimentally investigated in a JSR coupled with GC analysis at temperatures from 300 to 1000 K under O_3 addition of 1000 and 2000 ppm. The evolution with temperatures of the mole fraction of eight species was reported. The addition of O_3 enhanced the production of formaldehyde (CH_2O), methanol (CH_3OH), acetaldehyde (CH_3CHO), oxirane (C_2H_4O), formic acid (HCOOH), CO, and CO_2. This work also demonstrates that the initial ozonolysis reaction shifts the temperature window of the conversion of C_2H_4 and product formation to a lower temperature regime, in which the traditional C_2H_4 oxidation cannot be initiated. However, the major role of the O_3 addition in the oxidation of C_2H_4 remains limited since the additional conversion of C_2H_4 is below 10% with the initial mole fraction of O_3 used in this work and it does not change the chemistry of the high temperature regime. Nonetheless CH_2O, which is an important atmospheric pollutant, is the main product of the low-temperature ozonolysis reaction with a significant mole fraction ~1000 ppm. This quantitative result is important to consider especially for closed environments such as warehouses or fruit stores, where non-negligible

amounts of C_2H_4 can be present [54]. If these places use air purifiers, a phenomenon that is growing lately because of COVID-19, then a significant amount of formaldehyde can be expected, as many indoor appliances have been shown to generate significant amounts of O_3 [55]. More generally, the quantification of oxidation products and stable intermediates under conditions relevant to atmospheric and combustion studies provides a database of temperature-dependent products that can be used as a valuable guidance for future validation and improvement of detailed chemical kinetic models.

It has been shown that the configuration of the experimental setup and especially the mixing gas lines is important if one wants accurate quantitative ozonolysis experiments and avoid any thermal degradation of O_3 before reacting with the fuel. The experimental data were confronted to a kinetic model with an implemented ozone/ozonolysis submechanism based on IUPAC recommendations. Overall, contrary to what was mentioned in the literature, a kinetic model based on global reactions of the ethylene ozonolysis accurately reproduces the conversion of C_2H_4, O_3, and main products over a wide temperature range from 300 K to 1000 K. The kinetic model is able to capture the trend of the mole fraction profile of the small products above 800K, but below this temperature, disagreements between experiments and simulations are noted. The disagreements are also slightly worse at 2000 ppm than at 1000 ppm of O_3. This demonstrates that the implementation of a higher level of detail is needed in the kinetic model with further intermediate pathways to predict the entire product distribution derived from the C_2H_4 ozonolysis chemistry. However, this is beyond the scope of the current study because this would require a total remodeling of the current kinetic model which is based on a global approach of the ozonolysis process. For this, it would be necessary to have information on the kinetics and products of all the main and secondary reactions of the CI network. For example, the formation of methanol is difficult to intuit because the structure is different from the initial reactant. Due to its formation at low temperature, it is likely to be formed from dissociation reactions following the formation of CI. Rousso et al. [39] also detected methanol and mentioned that its formation is difficult to address because it could come from several pathways. The improvement of the knowledge of the C_2H_4 ozonolysis reaction network would benefit first from a fine identification of the elusive intermediates, which could not be detected in this work, to provide hints on the missing reaction pathways using for instance advanced spectroscopic techniques, such as PEPICO coupled with tunable photoionization sources.

ACKNOWLEDGMENTS

No acknowledgements.

REFERENCES

[1] R. Criegee, G. Wenner, Die Ozonisierung des 9,10-Oktalins, Justus Liebigs Annalen Der Chemie. 564 (1949) 9–15. https://doi.org/10.1002/jlac.19495640103.

[2] R. Huisgen, Kinetics and Mechanism of 1,3-Dipolar Cycloadditions, Angewandte Chemie International Edition in English. 2 (1963) 633–645. https://doi.org/10.1002/anie.196306331.

[3] L. Vereecken, A. Novelli, D. Taraborrelli, Unimolecular decay strongly limits the atmospheric impact of Criegee intermediates, Phys. Chem. Chem. Phys. 19 (2017) 31599–31612. https://doi.org/10.1039/C7CP05541B.

[4] R. L. Caravan, M.A. H. Khan, B. Rotavera, E. Papajak, I. O. Antonov, M.-W. Chen, K. Au, W. Chao, D. L. Osborn, J. Jr-Min Lin, C. J. Percival, D. E. Shallcross, C. A. Taatjes, Products of Criegee intermediate reactions with NO 2 : experimental measurements and tropospheric implications, Faraday Discussions. 200 (2017) 313–330. https://doi.org/10.1039/C7FD00007C.

[5] M. Ehn, J.A. Thornton, E. Kleist, M. Sipilä, H. Junninen, I. Pullinen, M. Springer, F. Rubach, R. Tillmann, B. Lee, F. Lopez-Hilfiker, S. Andres, I.-H. Acir, M. Rissanen, T. Jokinen, S. Schobesberger, J. Kangasluoma, J. Kontkanen, T. Nieminen, T. Kurtén, L.B. Nielsen, S. Jørgensen, H.G. Kjaergaard, M. Canagaratna, M.D. Maso, T. Berndt, T. Petäjä, A. Wahner, V.-M. Kerminen, M. Kulmala, D.R. Worsnop, J. Wildt, T.F. Mentel, A large source of low-volatility secondary organic aerosol, Nature. 506 (2014) 476–479. https://doi.org/10.1038/nature13032.

[6] B. Yang, P. Ma, J. Shu, P. Zhang, J. Huang, H. Zhang, Formation mechanism of secondary organic aerosol from ozonolysis of gasoline vehicle exhaust, Environmental Pollution. 234 (2018) 960–968. https://doi.org/10.1016/j.envpol.2017.12.048.

[7] Y. Ju, J.K. Lefkowitz, C.B. Reuter, S.H. Won, X. Yang, S. Yang, W. Sun, Z. Jiang, Q. Chen, Plasma Assisted Low Temperature Combustion, Plasma Chem Plasma Process. 36 (2016) 85–105. https://doi.org/10.1007/s11090-015-9657-2.

[8] Y. Ju, W. Sun, Plasma assisted combustion: Dynamics and chemistry, Progress in Energy and Combustion Science. 48 (2015) 21–83. https://doi.org/10.1016/j.pecs.2014.12.002.

[9] S. Wenting, J. Yiguang, Nonequilibrium Plasma-Assisted Combustion: A Review of Recent Progress, (2013) 12.

[10] S. Starikovskaia, D.A. Lacoste, G. Colonna, Non-equilibrium plasma for ignition and combustion enhancement, Eur. Phys. J. D. 75 (2021) 231. https://doi.org/10.1140/epjd/s10053-021-00240-2.

[11] A. Starikovskiy, N. Aleksandrov, Plasma-assisted ignition and combustion, Progress in Energy and Combustion Science. 39 (2013) 61–110. https://doi.org/10.1016/j.pecs.2012.05.003.

[12] W. Sun, X. Gao, B. Wu, T. Ombrello, The effect of ozone addition on combustion: Kinetics and dynamics, Progress in Energy and Combustion Science. 73 (2019) 1–25. https://doi.org/10.1016/j.pecs.2019.02.002.

[13] X. Gao, Y. Zhang, S. Adusumilli, J. Seitzman, W. Sun, T. Ombrello, C. Carter, The effect of ozone addition on laminar flame speed, Combustion and Flame. 162 (2015) 3914–3924. https://doi.org/10.1016/j.combustflame.2015.07.028.

[14] X. Gao, J. Zhai, W. Sun, T. Ombrello, C.D. Carter, The Effect of Ozone Addition on Autoignition and Flame Stabilization, in: 54th AIAA Aerospace Sciences Meeting, American Institute of Aeronautics and Astronautics, San Diego, California, USA, 2016. https://doi.org/10.2514/6.2016-0960.
[15] X. Gao, B. Wu, W. Sun, T. Ombrello, C. Carter, Ozonolysis activated autoignition in non-premixed coflow, J. Phys. D: Appl. Phys. 52 (2019) 105201. https://doi.org/10.1088/1361-6463/aaf785.
[16] A. Alfazazi, A. Al-Omier, A. Secco, H. Selim, Y. Ju, S.M. Sarathy, Cool diffusion flames of butane isomers activated by ozone in the counterflow, Combustion and Flame. 191 (2018) 175–186. https://doi.org/10.1016/j.combustflame.2017.12.034.
[17] T. Ombrello, S.H. Won, Y. Ju, S. Williams, Flame propagation enhancement by plasma excitation of oxygen. Part I: Effects of O3, Combustion and Flame. 157 (2010) 1906–1915. https://doi.org/10.1016/j.combustflame.2010.02.005.
[18] J.-B. Masurier, F. Foucher, G. Dayma, P. Dagaut, Investigation of iso-octane combustion in a homogeneous charge compression ignition engine seeded by ozone, nitric oxide and nitrogen dioxide, Proceedings of the Combustion Institute. 35 (2015) 3125–3132. https://doi.org/10.1016/j.proci.2014.05.060.
[19] S. Sayssouk, D. Nelson-Gruel, C. Caillol, P. Higelin, Y. Chamaillard, Towards control of HCCI combustion by ozone addition: a mathematical approach to estimate combustion parameters, IFAC-PapersOnLine. 49 (2016) 361–368. https://doi.org/10.1016/j.ifacol.2016.08.054.
[20] S. Ji, X. Lan, J. Lian, H. Xu, Y. Wang, Y. Cheng, Y. Liu, Influence of Ozone on Ignition and Combustion Performance of a Lean Methane/Air Mixture, Energy Fuels. 31 (2017) 14191–14200. https://doi.org/10.1021/acs.energyfuels.7b02389.
[21] D. Singleton, C. Carter, S.J. Pendleton, C. Brophy, J. Sinibaldi, J.W. Luginsland, M. Brown, E. Stockman, M.A. Gundersen, The effect of humidity on hydroxyl and ozone production by nanosecond discharges, Combustion and Flame. 167 (2016) 164–171. https://doi.org/10.1016/j.combustflame.2016.02.016.
[22] J.-B. Masurier, F. Foucher, G. Dayma, P. Dagaut, Homogeneous Charge Compression Ignition Combustion of Primary Reference Fuels Influenced by Ozone Addition, Energy Fuels. 27 (2013) 5495–5505. https://doi.org/10.1021/ef401009x.
[23] C.B. Reuter, T.M. Ombrello, Flame enhancement of ethylene/methane mixtures by ozone addition, Proceedings of the Combustion Institute. 38 (2021) 2397–2407. https://doi.org/10.1016/j.proci.2020.06.122.
[24] C.W. Gillies, J.Z. Gillies, R.D. Suenram, F.J. Lovas, E. Kraka, D. Cremer, Van der Waals complexes in 1,3-dipolar cycloaddition reactions: ozone-ethylene, ACS Publications. (2002). https://doi.org/10.1021/ja00007a010.
[25] J.Z. Gillies, C.W. Gillies, R.D. Suenram, F.J. Lovas, W. Stahl, The microwave spectrum and molecular structure of the ethylene-ozone van der Waals complex, ACS Publications. (2002). https://doi.org/10.1021/ja00190a056.
[26] L. Nord, Ozone complexes in solid nitrogen, Journal of Molecular Structure. 96 (1983) 37–44. https://doi.org/10.1016/0022-2860(82)90055-2.
[27] P.S. Bailey, J.A. Thompson, B.A. Shoulders, Structure of the Initial Ozone-Olefin Adduct, J. Am. Chem. Soc. 88 (1966) 4098–4099. https://doi.org/10.1021/ja00969a042.
[28] L.A. Hull, I.C. Hisatsune, J. Heicklen, Low-temperature infrared studies of simple alkene-ozone reactions, J. Am. Chem. Soc. 94 (1972) 4856–4864. https://doi.org/10.1021/ja00769a010.
[29] C.K. Kohlmiller, L. Andrews, Infrared spectrum of the primary ozonide of ethylene in solid xenon, J. Am. Chem. Soc. 103 (1981) 2578–2583. https://doi.org/10.1021/ja00400a016.
[30] H. Kuehne, H.H. Guenthard, Spectroscopic study of the ozone-ethylene reaction.

509 Matrix-infrared spectra of three isotopic ethylene ozonides, J. Phys. Chem. 80 (1976) 1238–
510 1247. https://doi.org/10.1021/j100552a025.
511 [31] M. Hawkins, C.K. Kohlmiller, L. Andrews, Matrix infrared spectra and photolysis and
512 pyrolysis of isotopic secondary ozonides of ethylene, J. Phys. Chem. 86 (1982) 3154–3166.
513 https://doi.org/10.1021/j100213a019.
514 [32] H.E. O'Neal, C. Blumstein, A new mechanism for gas phase ozone–olefin reactions,
515 International Journal of Chemical Kinetics. 5 (1973) 397–413.
516 https://doi.org/10.1002/kin.550050310.
517 [33] L.B. Harding, W.A. Goddard, Mechanisms of gas-phase and liquid-phase ozonolysis,
518 J. Am. Chem. Soc. 100 (1978) 7180–7188. https://doi.org/10.1021/ja00491a010.
519 [34] D.L. Osborn, C.A. Taatjes, The physical chemistry of Criegee intermediates in the gas
520 phase, International Reviews in Physical Chemistry. 34 (2015) 309–360.
521 https://doi.org/10.1080/0144235X.2015.1055676.
522 [35] C.A. Taatjes, Criegee Intermediates: What Direct Production and Detection Can Teach
523 Us About Reactions of Carbonyl Oxides, Annual Review of Physical Chemistry. 68 (2017)
524 183–207. https://doi.org/10.1146/annurev-physchem-052516-050739.
525 [36] C.C. Womack, M.-A. Martin-Drumel, G.G. Brown, R.W. Field, M.C. McCarthy,
526 Observation of the simplest Criegee intermediate CH_2OO in the gas-phase ozonolysis of
527 ethylene, Sci. Adv. 1 (2015) e1400105. https://doi.org/10.1126/sciadv.1400105.
528 [37] T.L. Nguyen, H. Lee, D.A. Matthews, M.C. McCarthy, J.F. Stanton, Stabilization of
529 the Simplest Criegee Intermediate from the Reaction between Ozone and Ethylene: A High-
530 Level Quantum Chemical and Kinetic Analysis of Ozonolysis, J. Phys. Chem. A. 119 (2015)
531 5524–5533. https://doi.org/10.1021/acs.jpca.5b02088.
532 [38] M. Pfeifle, Y.-T. Ma, A.W. Jasper, L.B. Harding, W.L. Hase, S.J. Klippenstein,
533 Nascent energy distribution of the Criegee intermediate CH2OO from direct dynamics
534 calculations of primary ozonide dissociation, J. Chem. Phys. 148 (2018) 174306.
535 https://doi.org/10.1063/1.5028117.
536 [39] A.C. Rousso, N. Hansen, A.W. Jasper, Y. Ju, Low-Temperature Oxidation of Ethylene
537 by Ozone in a Jet-Stirred Reactor, J. Phys. Chem. A. 122 (2018) 8674–8685.
538 https://doi.org/10.1021/acs.jpca.8b06556.
539 [40] A. C. Rousso, N. Hansen, A. W. Jasper, Y. Ju, Identification of the Criegee
540 intermediate reaction network in ethylene ozonolysis: impact on energy conversion strategies
541 and atmospheric chemistry, Physical Chemistry Chemical Physics. 21 (2019) 7341–7357.
542 https://doi.org/10.1039/C9CP00473D.
543 [41] N. Genossar, J. P. Porterfield, J. H. Baraban, Decomposition of the simplest
544 ketohydroperoxide in the ozonolysis of ethylene, Physical Chemistry Chemical Physics. 22
545 (2020) 16949–16955. https://doi.org/10.1039/D0CP02798G.
546 [42] X. Shen, X. Yang, J. Santner, J. Sun, Y. Ju, Experimental and kinetic studies of
547 acetylene flames at elevated pressures, Proceedings of the Combustion Institute. 35 (2015)
548 721–728. https://doi.org/10.1016/j.proci.2014.05.106.
549 [43] H. Zhao, J. Fu, F.M. Haas, Y. Ju, Effect of prompt dissociation of formyl radical on
550 1,3,5-trioxane and CH2O laminar flame speeds with CO2 dilution at elevated pressure,
551 Combustion and Flame. 183 (2017) 253–260.
552 https://doi.org/10.1016/j.combustflame.2017.05.005.
553 [44] H. Zhao, X. Yang, Y. Ju, Kinetic studies of ozone assisted low temperature oxidation
554 of dimethyl ether in a flow reactor using molecular-beam mass spectrometry, Combustion and
555 Flame. 173 (2016) 187–194. https://doi.org/10.1016/j.combustflame.2016.08.008.
556 [45] C.B. Reuter, T.M. Ombrello, S.G. Tuttle, Can ozonolysis reactions influence
557 detonations?, Shock Waves. 32 (2022) 363–371. https://doi.org/10.1007/s00193-022-01082-6.
558 [46] J. Bourgalais, O. Herbinet, H.-H. Carstensen, J. Debleza, G.A. Garcia, P. Arnoux, L.S.

Tran, G. Vanhove, B. Liu, Z. Wang, M. Hochlaf, L. Nahon, F. Battin-Leclerc, Jet-Stirred Reactor Study of Low-Temperature Neopentane Oxidation: A Combined Theoretical, Chromatographic, Mass Spectrometric, and PEPICO Analysis, Energy Fuels. 35 (2021) 19689–19704. https://doi.org/10.1021/acs.energyfuels.1c02080.
[47] R.J. Kee, F.M. Rupley, J.A. Miller, M.E. Coltrin, J.F. Grcar, E. Meeks, H.K. Moffat, A.E. Lutz, G. Dixon-Lewis, M.D. Smooke, CHEMKIN Collection, release 3.6; Reaction Design. Inc.; San Diego, CA, (2000).
[48] O. Herbinet, G. Dayma, Jet-Stirred Reactors, in: F. Battin-Leclerc, J.M. Simmie, E. Blurock (Eds.), Cleaner Combustion, Springer London, London, 2013: pp. 183–210. https://doi.org/10.1007/978-1-4471-5307-8_8.
[49] J.P. Senosiain, S.J. Klippenstein, J.A. Miller, Reaction of Ethylene with Hydroxyl Radicals: A Theoretical Study, J. Phys. Chem. A. 110 (2006) 6960–6970. https://doi.org/10.1021/jp0566820.
[50] J. Jian, H. Hashemi, H. Wu, A.W. Jasper, P. Glarborg, A reaction mechanism for ozone dissociation and reaction with hydrogen at elevated temperature, Fuel. 322 (2022) 124138. https://doi.org/10.1016/j.fuel.2022.124138.
[51] R.L. Caravan, M.A.H. Khan, J. Zádor, L. Sheps, I.O. Antonov, B. Rotavera, K. Ramasesha, K. Au, M.-W. Chen, D. Rösch, D.L. Osborn, C. Fittschen, C. Schoemaecker, M. Duncianu, A. Grira, S. Dusanter, A. Tomas, C.J. Percival, D.E. Shallcross, C.A. Taatjes, The reaction of hydroxyl and methylperoxy radicals is not a major source of atmospheric methanol, Nat Commun. 9 (2018) 4343. https://doi.org/10.1038/s41467-018-06716-x.
[52] J.-F. Müller, Z. Liu, V.S. Nguyen, T. Stavrakou, J.N. Harvey, J. Peeters, The reaction of methyl peroxy and hydroxyl radicals as a major source of atmospheric methanol, Nat Commun. 7 (2016) 13213. https://doi.org/10.1038/ncomms13213.
[53] P. Neeb, O. Horie, G.K. Moortgat, The Ethene−Ozone Reaction in the Gas Phase, J. Phys. Chem. A. 102 (1998) 6778–6785. https://doi.org/10.1021/jp981264z.
[54] C.G. Rao, Engineering for Storage of Fruits and Vegetables: Cold Storage, Controlled Atmosphere Storage, Modified Atmosphere Storage, Academic Press, 2015.
[55] H. Salonen, T. Salthammer, L. Morawska, Human exposure to ozone in school and office indoor environments, Environment International. 119 (2018) 503–514. https://doi.org/10.1016/j.envint.2018.07.012.